The First Improper Ferroelectric of 2D Multilayered Hybrid Perovskite Enabling Strong Tunable Polarization-Directed Second Harmonic Generation Effect

Yu Ma, Jiaqi Wang, Wuqian Guo, Shiguo Han, Jinlong Xu, Yi Liu, Lei Lu, Zhenda Xie,* Junhua Luo, and Zhihua Sun**

2D organometallic halide perovskites are recently emerging as a robust family of ferroelectrics, of which their inherent spontaneous polarization (P_s) endows fascinating quadratic nonlinear optical properties. However, up to date, few studies are reported to tune and control the second harmonic generation (SHG) effect in this ferroelectric branch. Herein, the first improper ferroelectric of 2D multilayered hybrid perovskites, $(IA)_2(EA)_2Pb_3Br_{10}$ (1, where IA is isoamylammonium and EA is ethylammonium), which exhibits a high Curie temperature (≈371 K) and biaxial ferroelectricity with P_s of 2.2 μC cm^{-2} is reported. Strikingly, its unique in-plane ferroelectricity allows strong tunable SHG properties under the polarized-light. That is, the maximum SHG signals are observed with polarized-light parallel to P_s, while the minimum SHG appears along the vertical direction. This SHG anisotropy creates an extremely large dichroism ratio of ≈12, as visualized by 2D color mapping, which is the record-high merit for this type of SHG systems. To the best knowledge, this is the first time to achieve tunable SHG effects through ferroelectric polarization. As a pioneering study, the coupling between the SHG effect and ferroelectricity paves a new direction of 2D hybrid perovskite ferroelectrics toward smart optical device applications.

1. Introduction

Ferroelectrics have been developed as an indispensable class of electroactive materials, which are characterized by reversible switching of spontaneous polarization (P_s) under external electric fields.[1–3] Generally, the inherent absence of inversion symmetry in ferroelectrics allows for diverse and intriguing physical properties, including pyroelectricity, piezoelectricity, and optical nonlinearity; all of these merits have been widely utilized for the high-performance electronic and optoelectronic devices, such as piezoelectric sensors, switchable diodes, and self-powered photodetectors.[4–6] Among them, second harmonic generation (SHG) is a typical optical nonlinearity that refers to the frequency doubling of intense incident laser pulses, which imposes an essential criteria of noncentrosymmetric crystal structure.[7] This crystallography requirement suggests that the intrinsic polarity of ferroelectrics will necessarily endows SHG effects, as verified in the known members of $LiNbO_3$, KH_2PO_4, and $KNbO_3$.[8–10] Emphatically, owing to the high sensitivity to the symmetry breaking, SHG has behaved as a promising indicator to probe the emergence of ferroelectric polarization. This unique characteristic derives from the concept that electric field induced by the intense pulses strongly couples with that of intrinsic ferroelectric P_s, hence leading to the controllable tuning of SHG properties. For example, temperature-dependent SHG behaviors have been well investigated in $SrTiO_3$, $BaTiO_3$, and $AgNa(NO_2)_2$,[11–13] closely related to the symmetry breaking upon temperature changing. Despite great efforts, these studies on temperature-dependent SHG effect are insufficient to elucidate its strong dependence on ferroelectric P_s. It remains a great challenge to establish tunable SHG effects through electric polarization not involving thermal stimulus, and thus to explore new ferroelectric candidates with modulated SHG effect are urgently demanded for assembling smart optoelectronic devices.

2D hybrid perovskites are recently booming as a promising class of optoelectronic materials that display the fascinating physical merits, including structure tunability, phase stability, quantum, and dielectric confinement effects.[14,15] In contrast to conventional oxide counterparts, this 2D family of hybrid perovskites take advantage of structural flexibilities to accommodate versatile organic moieties as spacing cation.[16] Structurally, a high-degree freedom of molecular motions for the flexible components plays a crucial role to the emergency of ferroelectric

Y. Ma, J. Wang, W. Guo, S. Han, Y. Liu, L. Lu, Prof. J. Luo, Prof. Z. Sun
State Key Laboratory of Structure Chemistry
Fujian Institute of Research on the Structure of Matter
Chinese Academy of Sciences
Fuzhou, Fujian 350002, China
E-mail: sunzhihua@fjirsm.ac.cn

Y. Ma, J. Wang, W. Guo, S. Han, Y. Liu, L. Lu, Prof. J. Luo, Prof. Z. Sun
Fujian Science and Technology Innovation Laboratory for Optoelectronic
Information of China
Fuzhou, Fujian 350108, China

Dr. J. Xu, Prof. Z. Xie
National Laboratory of Solid State Microstructures
School of Electronic Science and Engineering
Nanjing University
Nanjing 210093, China
E-mail: jlxu@nju.edu.cn; xiezhenda@nju.edu.cn

order, as well as the accompanying SHG properties.[17] As exemplified by a series of 2D hybrid perovskites, such as (cyclohexylammonium)$_2$PbBr$_4$, (C$_2$H$_5$NH$_3$)$_4$Pb$_3$Br$_{10}$, and (C$_4$H$_9$NH$_3$)$_2$(C$_2$H$_5$NH$_3$)$_2$Pb$_3$Br$_{10}$,[18–20] their temperature-dependent SHG behaviors are well consistent with that of P_s. Consequently, this unique coupling between ferroelectricity and SHG effect offer new possibilities to modulate optical nonlinearity, which might not be present in the classical nonlinear optical materials. Especially, the improper ferroelectrics undergo the phase transition with P_s as the secondary order parameter,[21–23] different form proper ferroelectrics whose P_s is the primary order parameter during phase transition. The dielectric constants of improper ferroelectric remain low in the vicinity of phase transition temperature, which is usually at least one order of magnitude lower than those of proper ones. The bistable property of improper ferroelectrics has provided an ideal platform to tune SHG properties through the polarity switching. Up to date, despite intensive studies on 2D hybrid perovskite ferroelectrics, it remains unexplored to tune SHG effects through their electric bistability. In this context, taking into consideration of the coupling between P_s and SHG effect, we attempted to design new 2D hybrid perovskite ferroelectric for modulating SHG attributes and promote the advance of new-generation optoelectronic devices.

Herein, we present the first improper ferroelectric in the family of 2D multilayered hybrid perovskites, (IA)$_2$(EA)$_2$Pb$_3$Br$_{10}$ (**1**, where IA is isoamylammonium and EA is ethylammonium),

which adopts the trilayered inorganic topology composed of the (PbBr$_6$)$_n$ sheets. It undergoes a ferroelectric-to-paraelectric phase transition at the Curie temperature (T_c) of ≈371 K, and demonstrates the biaxial ferroelectricity with P_s value of ≈2.2 μC cm^{-2}. Emphatically, the inherent in-plane electric polarizations of **1** result in tunable SHG activities by applying polarized-light. When the polarized-light direction is parallel to P_s, the maximum SHG effect is achieved, while the minimum SHG signal appears with the polarized-light being vertical to P_s. The visualized color mapping for this strong SHG anisotropy reveals a large dichroism ratio up to ≈12, exceeding the most of known 2D SHG systems. As far as we are aware, this is the first time to tune SHG effects through the coupling between ferroelectricity and optical nonlinearity, This work sheds light on the exploration of new ferroelectric materials toward smart optical device applications.

2. Results and Discussion

Yellow plate-like crystals of **1** were successfully grown from its saturated solutions by the temperature cooling method (Figure S1, Supporting Information), and the phase purity has been solidly verified by powder X-ray diffraction (Figure S2, Supporting Information). General structure lattice for **1** features a typical 2D <100>-oriented multilayered Ruddlesden–Popper perovskite architecture (**Figure 1**a), resembling that of inorganic
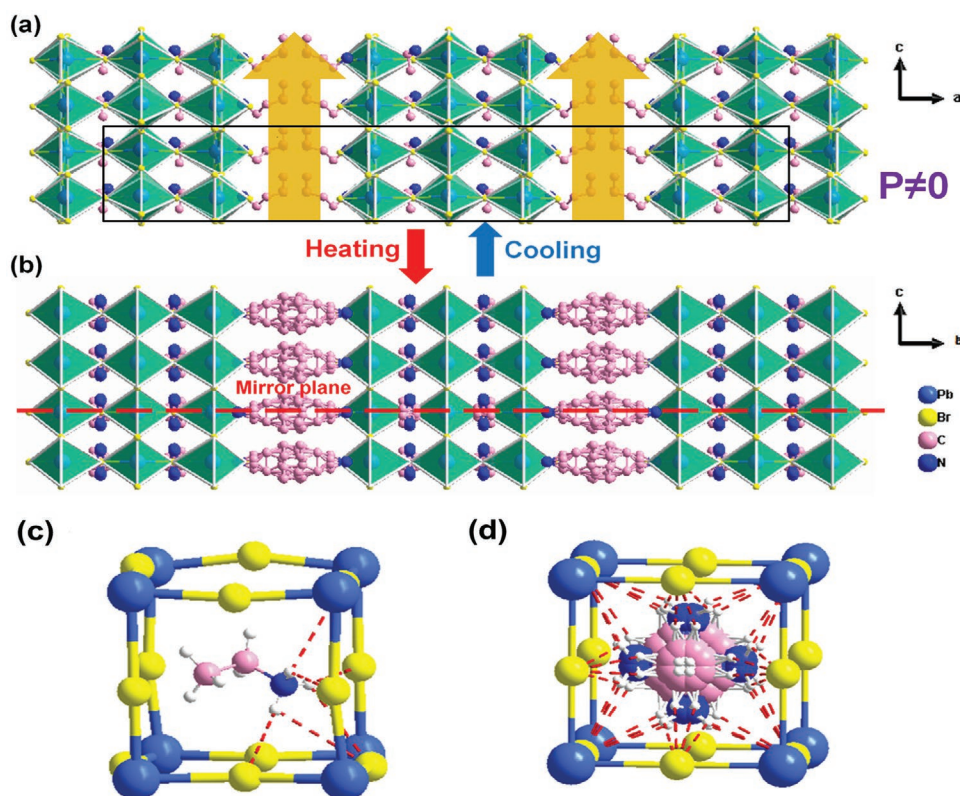
Figure 1. Crystal structure of **1** determined at different temperatures. a) Perspective view projected along the *b*-axis at 293 K. b) Perspective view projected along the *a*-axis at 383 K. The dash line represents the mirror plane. c,d) Diagram of the basic component for inorganic perovskite (Pb$_3$Br$_{10}$) frameworks at 293 and 383 K, respectively. The organic EA$^+$ cation inside the cavity undergoes the order-disorder structure change, and the distortion is also observed for the inorganic framework.

ADVANCED
SCIENCE NEWS
www.advancedsciencenews.com

ADVANCED
FUNCTIONAL
MATERIALS
www.afm-journal.de

oxide counterparts, such as $Sr_4Ti_3O_{10}$.[24] The inorganic perovskite $(Pb_3Br_{10})_n$ trilayers and spacing interlayers of organic IA^+ cations have an alternative arrangement along the <100>-orientation, with NH_3^+ moieties embedding inside the inorganic sheets via strong $N-H\cdots Br$ hydrogen bonds. The head-to-tail alignments of organic spacing cations result roughly in the (1/2 1/2) shift of adjacent perovskite blocks. This structural attribute is widely established with the large-size flexible organic cations filling the interlayer space. It is notable that the incorporation of organic EA^+ cations inside the perovskite cavities corresponds to the high-degree distortions of inorganic $PbBr_6$ octahedra. Depending on the flexible feature of spacing IA^+ cation, both in-plane and out-of-plane distortions are formed, (Figure S3, Supporting Information) as verified by the Pb—Br bond distances in the range of 2.931–3.151 Å. (Table S2, Supporting Information) From a dynamic perspective, the freedom for molecular motions of organic components affords a driving force to trigger phase transition, while the reorientation and tilting of $PbBr_6$ octahedra make a synergic cooperation to the generation of electric polarization.

Symmetry breaking of crystallography is indispensable for the emergence of ferroelectric polarization. Hence, we determined variable-temperature single crystal structures of 1 to confirm the occurrence of ferroelectric-to-paraelectric phase transition. At 293 K (below T_c, ferroelectric phase, FEP), its structure belongs to orthorhombic system with a polar space group $Cmc2_1$ (the point group $mm2$). The inorganic perovskite frameworks consist of infinite and staggered trilayers of $PbBr_6$ octahedra, interleaved by the spacing bilayers of organic IA^+ cations. In terms of electric polarization, the characteristic for this structure is that all the isoamyl groups of IA^+ cations arrange in a parallel order along the c-axis, and the similar alignment is also observed for the ethyl moieties of EA^+ cations. This parallel array suggests that the positive charge centers will shift along the c-axis direction. Meanwhile, the distortions and tilting motions of $PbBr_6$ octahedra (Figure 1c) also allow the relative displacement of negative charge centers. The separation of positive and negative charges thus favors the appearance of ferroelectric polarization in the c-axis direction.

At 383 K (above T_c, paraelectric phase, PEP), 1 belongs to a centrosymmetric space group $I4/mmm$ (the point group $4/mmm$) of which the cell constants are quite different from those of FEP (Table S1, Supporting Information). The most distinguishable change is that the organic cations become highly disordered at PEP, of which the atom occupancies at symmetry positions satisfy the crystallography criteria. As depicted in Figure 1b, the organic cations show serve orientational disorder with respect to the mirror plane, and the inorganic $PbBr_6$ octahedra also feature a highly symmetric motif (Figure 1d). The molecular dipole moment cancels each other out along the c-axis. Hence, the formation of polar structure and switchable electric polarization (e.g., ferroelectricity) could ascribe to the reorientation of organic cations through rotation between four equivalent sites. Our structure analysis confirms the symmetry breaking with an Aizu notation of $4/mmmFmm2$ in 1, stemming from the orientational ordering organic cations and the tilting of inorganic parts. The reduction of symmetry operation elements from 16 to 4 during the PE-to-FE phase transition

leads to four equivalent polarization directions, revealing the biaxial nature for ferroelectricity in 1,[25] as established by the following electric measurements.

Generally, the appearance of ferroelectricity is closely related to the symmetry breaking that results from temperature-induced structural phase transition.[26] Therefore, differential scanning calorimetry (DSC) and variable-temperature dielectric constant (ε') measurements were performed to verify the phase transition behaviors of 1. DSC trace clearly shows a pair of endothermic and exothermic peaks at 371/364 K during the heating and cooling runs (Figure 2a), revealing the occurrence of a reversible phase transition. The relatively large thermal hysteresis ($\Delta T \approx 7$ K) is reminiscent of the first-order characteristic for this phase transition. Figure 2b depicts the temperature-dependent ε' of 1 measured along three different crystallography axes of single crystal. The c-axis is the polar direction and parallel to inorganic perovskite sheets, while the a-axis direction is perpendicular to the inorganic layers (Figure 1a). The result discloses that ε' value exhibits obvious anomalies in the vicinity of T_c upon heating, which is well consistent with the DSC result, further confirming the structural change in 1. The anomaly magnitude of ε' has the crystallography anisotropy, that is, ε'_b and ε'_c values are larger than ε'_a.
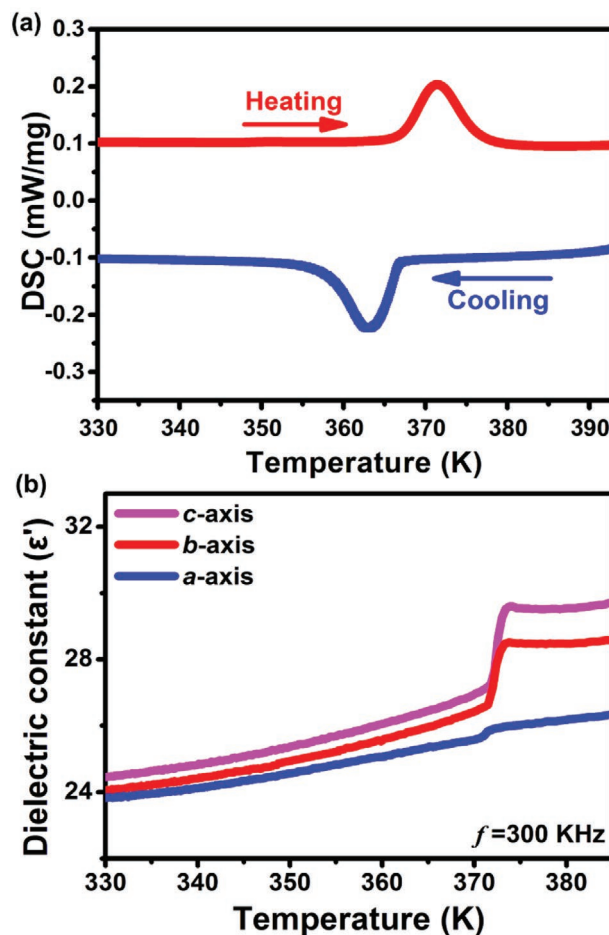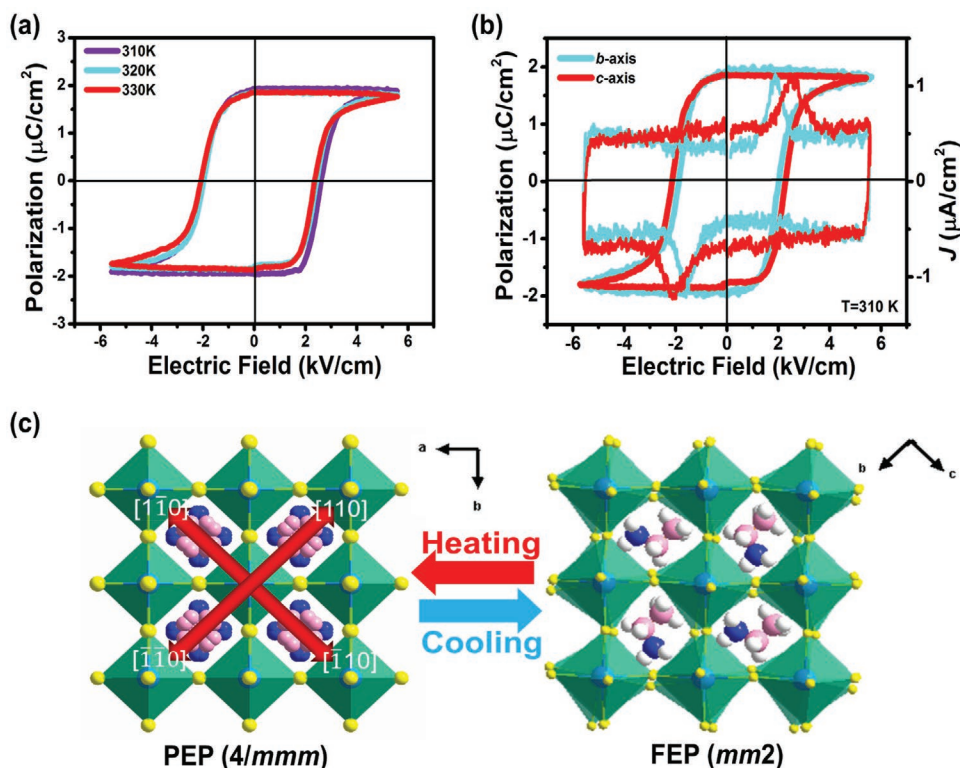

Figure 2. Phase transition behaviors of 1. a) DSC curves for 1. b) Temperature-dependence of dielectric constants measured along the a-,b-, and c-axes directions, respectively.
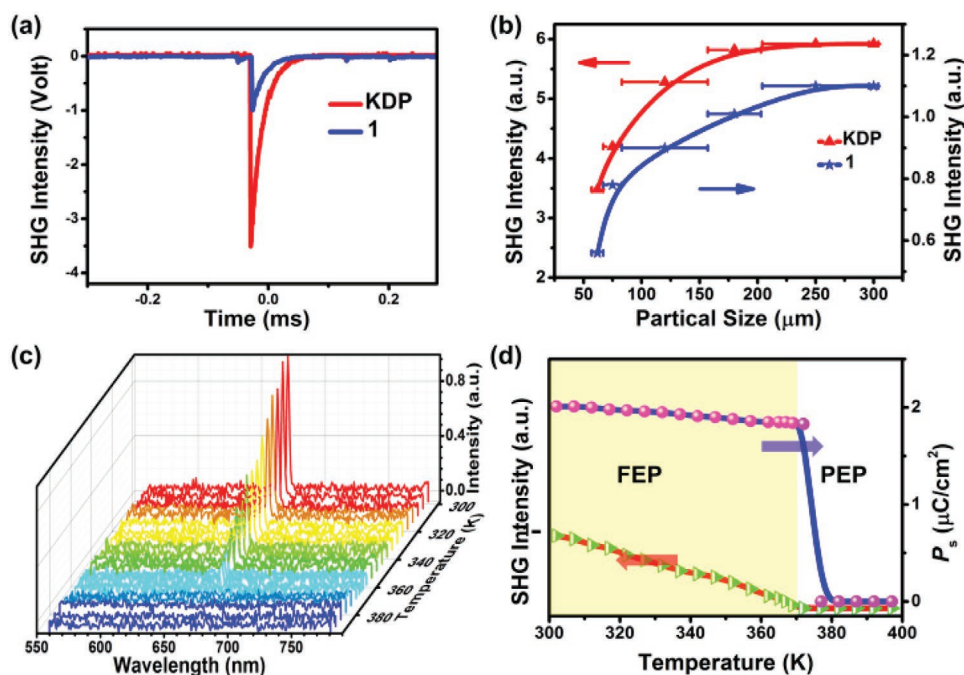
**ADVANCED
SCIENCE NEWS**

www.advancedsciencenews.com

**ADVANCED
FUNCTIONAL
MATERIALS**

www.afm-journal.de

Figure 3. Temperature-dependence and biaxial feature for ferroelectricity of **1**. a) *P–E* hysteresis loops measured along the *c*-axis via double-wave method at different temperatures. b) *P–E* hysteresis loops and related current density (*J–E*) traces collected along the *b*- and *c*-axes directions, revealing the biaxial characteristic. c) Symmetry breaking with an Aizu notation of 4/*mmmFmm*2 for **1**. There are four equivalent directions at PEP, as shown by the red arrowheads, which coincide fairly well with its crystallographic polar *c*-axis at FEP.

This is probably due to the dynamic motions of organic cations around the twofold axis. More strikingly, two plateaus of the temperature-dependent ε' are observed, and the presence of bistable dielectric states suggest that **1** might be an improper ferroelectric.[27,28] Although the bistable magnetic susceptibility has been widely observed in many systems, the dielectric bistability is still scarce for ferroelectrics. Such dielectric behaviors reveal great potentials of **1** for the next-generation smart electric devices, such as sensors, switches, and actuators.

For ferroelectrics, the reversible switching of polarization is an activated process that can be defined by the polarization versus electric field (*P–E*) hysteresis loops. Here, we used the double-wave method to determine the ferroelectric polarization reversal in **1** by recording the current density–electric field (*J–E*) curves. **Figure 3**a depicts the rectangular *P–E* hysteresis loops measured along the *c*-axis direction at different temperatures (Figure S4, Supporting Information). The P_s and coercive field (E_c) are derived to be 2.2 μC cm^{-2} and 2.5 kV cm^{-1}, respectively; this P_s value falls in the range of emerging molecular ferroelectrics, such as (*R*)-(-)-3-hydroxyquinuclidinium[29] and $(C_5H_9NH_3)CdCl_3$.[30] The E_c for reversing the electric polarization of **1** is much smaller than some organic ferroelectrics, such as croconic acid (E_c = 11–29 kV cm^{-1}) and benzimidazoles (E_c = 60–100 kV cm^{-1}),[31] probably due to the fact the spacing cations enable facile reorientation between inorganic perovskite sheets. It should be emphasized that the equivalent *P–E* hysteresis loops can be achieved not only along the *c*-axis but also

along the *b*-axis (Figure 3b), revealing the biaxial nature of the ferroelectricity in **1**. This feature stems from the electric-induced alteration of polarization axis in the multiaxial ferroelectrics. Crystallography analyses have presented the occurrence of symmetry breaking with an Aizu notation of 4/*mmmFmm*2 in **1**, giving rise to four equivalent directions of [$\bar{1}$10], [$\bar{1}\bar{1}$0], [110], and [1$\bar{1}$0] that coincide with its polar *c*-axis at FEP (Figure 3c). Above the T_c, in the paraelectric phase (PEP), **1** was transformed to the nonpolar space group of *I*4/*mmm* (point group of 4/*mmm*). The anisotropy of the *P–E* hysteresis loops of **1** is consistent with its biaxial characteristics, making it significantly different from the previously reported uniaxial ferroelectrics.

Considering that **1** crystallizes in the polar space group *Cmc*2$_1$ at FEP, it is expected to be SHG-active. At room temperature, **1** exhibits an obvious SHG effect with the signal intensity of ≈0.33 times as large as that of KDP (K$_2$HPO$_4$, **Figure 4**a). As shown in Figure 4b, the SHG intensities for **1** increase with the increasing of particle sizes and gradually reach the maximum. According to the rule proposed by Kurtz and Perry, this behavior suggests that **1** should be a phase-matching NLO material.[32] Particularly, the SHG signals of **1** exhibit the temperature-dependent tendency, as depicted in Figure 4c. At the PEP ($T > T_c$), there is no SHG signals observed for **1**, which agrees with its centrosymmetric space group of *I*4/*mmm*. With the temperature decreasing below 371 K ($T < T_c$), however, the SHG effect becomes active and the gradual increasing of SHG intensity coincides well with the polar structure at FEP.

ADVANCED
SCIENCE NEWS
www.advancedsciencenews.com

ADVANCED
FUNCTIONAL
MATERIALS
www.afm-journal.de

Figure 4. Nonlinear optical properties of **1**. a) SHG signals compared with the KH_2PO_4 reference. b) SHG intensities versus the particle size curves, revealing the phase-matching attribute. The solid curves are drawn to guide the eyes. c) Measurement of SHG signals at different temperatures. d) Temperature dependence of the SHG intensities and P_s, almost exhibiting a similar variation tendency.

According to Landau theory, the temperature dependence of SHG effects in ferroelectric materials is basically consistent with that of P_s, following the linear relationship of $\chi^{(2)} = 6\varepsilon_0 b P_s$, where $\chi^{(2)}$ is SHG coefficient and b is the temperature-independent constant.[33] Figure 4d depicts the variations of SHG signals and P_s for **1** at different temperatures, and both of them disappear with temperature rising beyond the T_c. Such thermal behaviors of SHG performances solidly confirm the symmetry breaking for **1** during its phase transition process.

Regarding the close relationship between P_s and SHG effect, we further attempt to achieve the tunable SHG properties based on ferroelectricity under the polarized-light (Figure S5, Supporting Information). Single crystals of **1** with the well-developed (100) crystal face were fixed, and the high-intense fundamental laser was incident along the a-axis direction. By rotating the polarizer in the range from 0° to 360°, the incident-light direction can be polarized (**Figure 5**a), of which the 0° and 90° polarization angles correspond to the c-axis and b-axis directions, respectively. Figure 5b displays the tunable angle-resolved SHG signals of **1** in the polar coordinate, which exhibit dramatic variations as a function of polarization angle. The findings indicate that the maximum SHG responses emerge at 0° and 180° polarization, corresponding to the laser polarized along its polar c-axis (parallel to P_s). In contrast, the SHG intensities drop to the minimum as the laser polarized parallel to b-axis (at 90° and 270°, vertical to P_s). The dichroism ratio between the maximum and minimum SHG signals are estimated to be ≈12, exceeding the recently emerging non-linear materials, such as Azobenzene SAM and β-[(MQ)ZnCl_3] (Figure 5c).[34–41] Besides, we can facilely control and tune its SHG effects by regulating the polarization-angles of incident laser. As far as we are aware, this is the first time to achieve

tunable SHG properties in 2D multilayered hybrid perovskite ferroelectrics, behaving as an evidence to the strong coupling between the SHG effect and ferroelectricity.

Furthermore, the evolutions of SHG intensities under different incident laser energy are plotted with respect to polarization angles in the polar coordinate. The stronger SHG signals are observed under higher laser energy, and their fittings present a typical cosine function (Figure 5b), further disclosing the tunability of SHG attributes in **1**. Figure 5d depicts the 2D color mapping of the polarization-directed SHG signals for **1**. It is clearly demonstrated that the strongest SHG intensities emerge with the incident laser polarized at 0° and 180°, while the weakest signals are observed at 90° and 270°. The large contrast for SHG intensities is also reminiscent of its polarization-directed anisotropy, coinciding with the experimental SHG data in Figure 5b. Such findings possibly provide a new direction for the applications of hybrid perovskite ferroelectrics in the field of nonlinear optics.

3. Conclusion

In summary, we have presented a new improper ferroelectric of 2D hybrid perovskites, $(IA)_2(EA)_2Pb_3Br_{10}$, which exhibits the fascinating ferroelectricity with a high T_c and biaxial P_s. For the first time, the rational tuning of SHG effects has been achieved by applying the polarized-light, closely involving with its intrinsic in-plane electric polarization. The maximum SHG effect is established with the polarized-light direction parallel to P_s, while the minimum appears in the vertical direction. Through the visualized 2D color mapping, its strong SHG anisotropy enables an extremely large
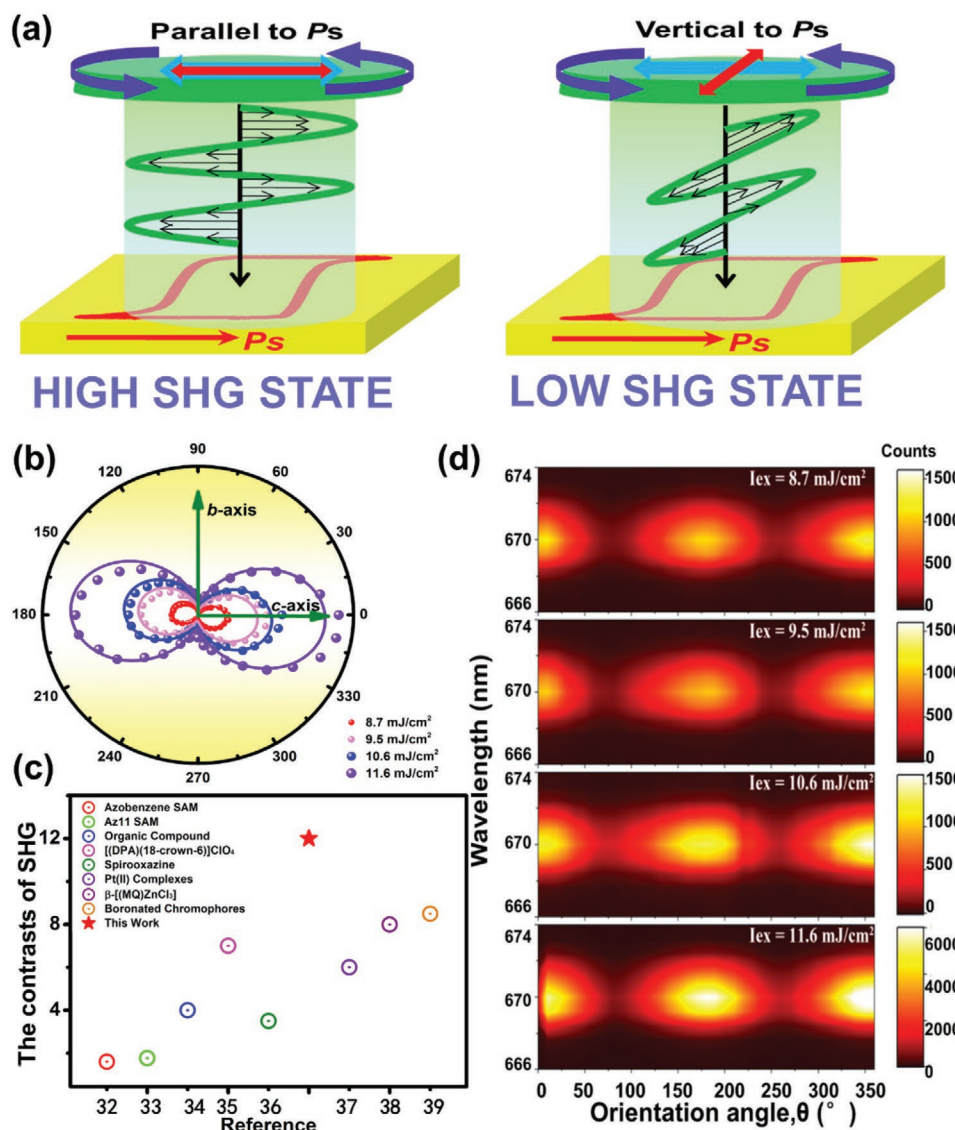
Figure 5. Properties of tunable SHG effect. a) Schematic illustration for tuning SHG properties of **1** under the polarized light. b) Tunable SHG results as a function of polarization angle under different laser energy. The dots and lines are experimental data and the fitting curves, respectively. c) Compared the SHG contrast of this work and the literature. d) Visualized 2D color mapping for the switchable SHG intensities.

dichroism ratio of ≈12, exceeding the recently emerging molecular ferroelectric materials. The coupling between SHG effect and ferroelectricity offers new possibilities to modulate optical nonlinearities that will not be present in the classical nonlinear optical materials. This work sheds light on a new direction of 2D hybrid perovskite ferroelectrics toward optoelectronic device applications.

(CCDC 2054331, 2054332 contain the supplementary crystallographic data for this paper. These data can be obtained free of charge from The Cambridge Crystallographic Data Centre via www.ccdc.cam.ac.uk/data_request/cif.)

Supporting Information

Supporting Information is available from the Wiley Online Library or from the author.

Conflict of Interest

The authors declare no conflict of interest.

Data Availability Statement

Research data are not shared.

[1] C. K. Yang, W. N. Chen, Y. T. Ding, J. Wang, Y. Rao, W. Q. Liao, Y. Y. Tang, P. F. Li, Z. X. Wang, R. G. Xiong, *Adv. Mater.* **2019**, *31*, 1808088.

[2] P. P. Shi, S. Q. Lu, X. J. Song, X. G. Chen, W. Q. Liao, P. F. Li, Y. Y. Tang, R. G. Xiong, *J. Am. Chem. Soc.* **2019**, *141*, 18334.

[3] C. Shi, L. Ye, Z. X. Gong, J. J. Ma, Q. W. Wang, J. Y. Jiang, M. M. Hua, C. F. Wang, H. Yu, Y. Zhang, H. Y. Ye, *J. Am. Chem. Soc.* **2020**, *142*, 545.

[4] W.-J. Xu, S. Kopyl, A. Kholkin, J. Rocha, *Coord. Chem. Rev.* **2019**, *387*, 398.

[5] C. Paillard, X. Bai, I. C. Infante, M. Guennou, G. Geneste, M. Alexe, J. Kreisel, B. Dkhil, *Adv. Mater.* **2016**, *28*, 5153.

[6] I.-H. Park, K. C. Kwon, Z. Zhu, X. Wu, R. Li, Q.-H. Xu, K. P. Loh, *J. Am. Chem. Soc.* **2020**, *142*, 18592.

[7] K. W. DeLong, R. Trebino, J. Hunter, W. E. White, *J. Opt. Soc. Am. B* **1994**, *11*, 2206.

[8] M. Yamada, N. Nada, M. Saitoh, K. Watanabe, *Appl. Phys. Lett.* **1993**, *62*, 435.

[9] M. I. Baig, M. Anis, G. G. Muley, *Opt. Mater.* **2017**, *72*, 1.

[10] V. Gopalan, R. Raj, *Appl. Phys. Lett.* **1996**, *68*, 1323.

[11] R. C. Haislmaier, R. Engel-Herbert, V. Gopalan, *Appl. Phys. Lett.* **2016**, *109*, 032901.

[12] A. M. Pugachev, V. I. Kovalevskii, N. V. Surovtsev, S. Kojima, S. A. Prosandeev, I. P. Raevski, S. I. Raevskaya, *Phys. Rev. Lett.* **2012**, *108*, 247601.

[13] A. V. Kityk, R. Czaplicki, A. Klöpperpieper, A. S. Andrushchak, B. Sahraoui, *Appl. Phys. Lett.* **2010**, *96*, 061911.

[14] S. Han, X. Liu, Y. Liu, Z. Xu, Y. Li, M. Hong, J. Luo, Z. Sun, *J. Am. Chem. Soc.* **2019**, *141*, 12470.

[15] Y. Ma, J. Wang, Y. Liu, S. Han, Y. Li, Z. Xu, W. Guo, J. Luo, M. Hong, Z. Sun, *J. Mater. Chem. C* **2021**, *9*, 881.

[16] G. Grancini, M. K. Nazeeruddin, *Nat. Rev. Mater.* **2018**, *4*, 4.

[17] W. Q. Liao, Y. Zhang, C. L. Hu, J. G. Mao, H. Y. Ye, P. F. Li, S. D. Huang, R. G. Xiong, *Nat. Commun.* **2015**, *6*, 7338.

[18] Z. Sun, X. Liu, T. Khan, C. Ji, M. A. Asghar, S. Zhao, L. Li, M. Hong, J. Luo, *Angew. Chem., Int. Ed.* **2016**, *55*, 6545.

[19] S. Wang, X. Liu, L. Li, C. Ji, Z. Sun, Z. Wu, M. Hong, J. Luo, *J. Am. Chem. Soc.* **2019**, *141*, 7693.

[20] C. Ji, S. Wang, Y. Wang, H. Chen, L. Li, Z. Sun, Y. Sui, S. Wang, J. Luo, *Adv. Funct. Mater.* **2019**, *30*, 1905529.

[21] V. Dvořák, *Ferroelectrics* **1974**, *7*, 1.

[22] N. A. Benedek, C. J. Fennie, *Phys. Rev. Lett.* **2011**, *106*, 107204.

[23] Z. S. Y. Tang, S. Zhang, C. Ji, T. Chen, J. Luo, *Adv. Mater.* **2015**, *27*, 4795.

[24] S. N. Ruddlesden, P. Popper, *Acta Crystallogr.* **1958**, *11*, 54.

[25] K. Aizu, *J. Phys. Soc. Jpn.* **1969**, *27*, 387.

[26] W.-J. Xu, C.-T. He, C.-M. Ji, S.-L. Chen, R.-K. Huang, R.-B. Lin, W. Xue, J.-H. Luo, W.-X. Zhang, X.-M. Chen, *Adv. Mater.* **2016**, *28*, 5886.

[27] Y. Zhang, H.-Y. Ye, H.-L. Cai, D.-W. Fu, Q. Ye, W. Zhang, Q. Zhou, J. Wang, G.-L. Yuan, R.-G. Xiong, *Adv. Mater.* **2014**, *26*, 4515.

[28] E. Bousquet, M. Dawber, N. Stucki, C. Lichtensteiger, P. Hermet, S. Gariglio, J.-M. Triscone, P. Ghosez, *Nature* **2008**, *452*, 732.

[29] P.-F. Li, Y.-Y. Tang, Z.-X. Wang, H.-Y. Ye, Y.-M. You, R.-G. Xiong, *Nat. Commun.* **2016**, *7*, 13635.

[30] K. Gesi, *J. Phys. Soc. Jpn.* **1990**, *59*, 432.

[31] S. Horiuchi, Y. Tokura, *Nat. Mater.* **2008**, *7*, 357.

[32] S. K. Kurtz, T. T. Perry, *J. Appl. Phys.* **1968**, *39*, 3798.

[33] B. I. Halperin, P. A. Lee, N. Read, *Phys. Rev. B* **1993**, *47*, 7312.

[34] M. Schulze, M. Utecht, T. Moldt, D. Przyrembel, C. Gahl, M. Weinelt, P. Saalfrank, P. Tegeder, *Phys. Chem. Chem. Phys.* **2015**, *17*, 18079.

[35] C. Tonnelé, B. Champagne, L. Muccioli, F. Castet, *Chem. Mater.* **2019**, *31*, 6759.

[36] S. van Bezouw, J. Campo, S.-H. Lee, O. P. Kwon, W. Wenseleers, *J. Phys. Chem. C* **2015**, *119*, 21658.

[37] C. Ji, Z. Sun, S. Zhang, S. Zhao, T. Chen, Y. Tang, J. Luo, *Chem. Commun.* **2015**, *51*, 2298.

[38] J. Yuan, J. Yuan, X. Tian, J. Sun, Y. Ge, *J. Phys. Chem. C* **2016**, *120*, 14840.

[39] J. Boixel, V. Guerchais, H. L.e Bozec, D. Jacquemin, A. Amar, A. Boucekkine, A. Colombo, C. Dragonetti, D. Marinotto, D. Roberto, S. Righetto, R. De Angelis, *J. Am. Chem. Soc.* **2014**, *136*, 5367.

[40] X.-S. Xing, R.-J. Sa, P.-X. Li, N.-N. Zhang, Z.-Y. Zhou, B.-W. Liu, J. Liu, M.-S. Wang, G.-C. Guo, *Chem. Sci.* **2017**, *8*, 7751.

[41] C. Jiménez, N. Farfan, M. Romero-Avila, R. Santillan, I. Malfant, P. G. Lacroix, *J. Organomet. Chem.* **2015**, *799*, 215.